AD-A193 698 ELASTIC BEHAVIOR OF A RUBBER LAYER BONDED BETWEEN TWO RIGID SPHERES(U) AKRON UNIV OH INST OF POLYMER SCIENCE A N GENT ET AL. MAY 88 TR-15 N00014-85-K-0222 1/1

UNCLASSIFIED F/G 11/10 NL

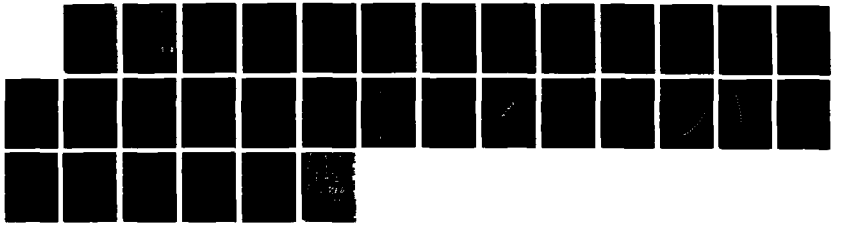

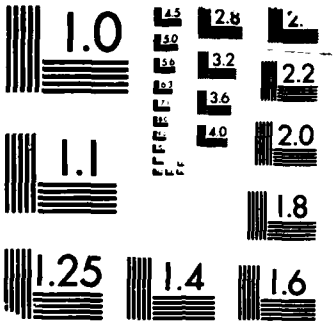

OFFICE OF NAVAL RESEARCH

Contract: N00014-85-K-0222

Work Unit: 4327-555

Scientific Officer: Dr. Richard S. Miller

Technical Report No. 15

ELASTIC BEHAVIOR OF A RUBBER LAYER BONDED BETWEEN TWO RIGID SPHERES

by

A. N. Gent and Y.-C. Hwang

Institute of Polymer Science
The University of Akron
Akron, Ohio 44325

May, 1988

SECURITY CLASSIFICATION OF THIS PAGE (When Data Entered)

REPORT DOCUMENTATION PAGE

READ INSTRUCTIONS BEFORE COMPLETING FORM

1. REPORT NUMBER: Technical Report No. 15	2. GOVT ACCESSION NO.
3. RECIPIENT'S CATALOG NUMBER	
4. TITLE (and Subtitle): Elastic Behavior of a Rubber Layer Bonded Between Two Rigid Spheres	5. TYPE OF REPORT & PERIOD COVERED: Technical Report
6. PERFORMING ORG. REPORT NUMBER	
7. AUTHOR(s): A. N. Gent and Y.-C. Hwang	8. CONTRACT OR GRANT NUMBER(s): N00014-85-K-0222
9. PERFORMING ORGANIZATION NAME AND ADDRESS: Institute of Polymer Science, The University of Akron, Akron, Ohio 44325	10. PROGRAM ELEMENT, PROJECT, TASK AREA & WORK UNIT NUMBERS: 4327-555
11. CONTROLLING OFFICE NAME AND ADDRESS: Office of Naval Research, Power Program, Arlington, VA 22217-5000	12. REPORT DATE: May 1988
	13. NUMBER OF PAGES: 29
14. MONITORING AGENCY NAME & ADDRESS (if different from Controlling Office)	15. SECURITY CLASS. (of this report): Unclassified
	15a. DECLASSIFICATION/DOWNGRADING SCHEDULE

16. DISTRIBUTION STATEMENT (of this Report)

According to attached distribution list.
Approved for public release; distribution unrestricted.

17. DISTRIBUTION STATEMENT (of the abstract entered in Block 20, if different from Report)

18. SUPPLEMENTARY NOTES

Submitted for publication in: Rubber Chemistry and Technology

19. KEY WORDS (Continue on reverse side if necessary and identify by block number)

Cracking, Composites, Compressibility, Deformation, Dilatancy, Elasticity, Elastomers, Failure, Fracture, Particles, Reinforcement, Rubber, Stress Analysis.

20. ABSTRACT (Continue on reverse side if necessary and identify by block number)

Finite element methods (FEM) have been employed to calculate the stresses set up in a thin rubber layer, bonded between two rigid spheres, when small tensile or compressive deflections are imposed. Values of stiffness have been calculated for various spacings of the spheres, i.e.,

DD FORM 1 JAN 73 1473 EDITION OF 1 NOV 65 IS OBSOLETE
S/N 0102-LF-014-6601

SECURITY CLASSIFICATION OF THIS PAGE (When Data Entered)

20. ABSTRACT (continued)

for various thicknesses of the rubber layer. They are in good agreement with earlier experimental measurements of compression stiffness and with the predictions of an approximate theoretical treatment (1). However, they are strongly affected by small departures of the rubber layer from complete incompressibility. The highest dilatant stress (in tension) is found to be set up on the central axis, near the bonded surfaces, where internal failure has been observed to occur in similar bonded layers (2). For moderately thick layers, the axial tensile stress in the center of the layer is substantially higher than the lateral stresses. This feature suggests that the initiation of failure in this location may not obey the same criterion as for an isotropic stress field, and that a crack, once formed here, will propagate as a tear across the axis of symmetry.

Introduction

The elastic behavior of a rubber layer sandwiched between, and bonded to, two rigid spherical surfaces is of interest for at least two reasons. Structures of this type are used as flexible mounts and cushioning devices, and design engineers need to be able to estimate the stiffness and the stresses set up within them. And they constitute a model of particle-filled composites, in which spherical particles are dispersed in a softer elastic medium. In this case a knowledge of the stiffness and stress distribution may provide insights into the phenomenon of reinforcement.

Elastic behavior under small compressions (and, equivalently, under small tensile deformations) has been analyzed previously, using some rather drastic approximations (1). The rubber was assumed to be linearly-elastic and incompressible in bulk, and the compressive force was assumed to consist of two terms : one due to simple compression of the layer, and a second arising from a hydrostatic pressure $\underline{P}$ set up as a result of the restraints at the bonded surfaces, where $\underline{P}$ was a function only of the lateral distance of a point in the layer from the central axis of the system. We now present a more detailed and accurate study of the stresses and deformations set up by compression or extension of the layer, using finite element methods (FEM) and not invoking the condition of incompressibility. Instead, values of Poisson's ratio lying between 0.45 and 0.5 have been employed, covering the widest range likely to be encountered with rubber formulations. A typical rubber vulcanizate has a value of Young's

(tensile) modulus $\underline{E}$ between about 2 and about 10 MPa, and a much larger modulus $\underline{K}$ of bulk compression, of about 1.1 GPa (3). Thus, Poisson's ratio ν, given by

$$\nu = (1/2) - E/6K \qquad (1)$$

ranges from about 0.4985 for relatively stiff compounds to about 0.4997 for relatively soft ones.

In addition, the distribution of pressure throughout the thickness of the rubber layer has been calculated, whereas, before, the approximate theory only yielded a uniform value.

These results have implications for the mode of fracture both of bonded rubber layers and of filled rubber and other particulate composites. Failure of rubber is known to take place where, and when, a triaxial tension (negative hydrostatic pressure) is set up that exceeds a critical value, given by about $\underline{5E/6}$, where $\underline{E}$ is Young's modulus (4-6). Under these circumstances, any small spherical cavity that is present within the rubber will expand indefinitely, i.e., until the rubber around it reaches its maximum extensibility. Then the rubber will tear open to create a large internal crack. Thus, a crucial question for elastomeric composites is : Under what circumstances and at what locations is this critical state likely to be reached ?

A second question is : In what direction will the crack, once formed, tend to propagate ? If it grows across the sample, then it will result in rupture. If, on the other hand, it grows parallel to the axis of the sample, then it will not necessarily lead to rupture.

Some preliminary conclusions on these points are reached here on the basis of the calculated stress distributions.

2. Finite Element Analysis

A sketch of the model structure is shown in Figure 1. Stress distributions within the rubber layer were calculated using the ADINA code (7), assuming that the structure was cylindrically symmetrical, and that the rubber was linearly-elastic, isotropic, and nearly incompressible in bulk, with values of Poisson's ratio, $\underline{\nu}$, between 0.45 and 0.4999. The two spheres were made effectively rigid by giving them a value of Young's modulus of 10^9 times that of the rubber.

Ten equal elements were employed vertically, between the surface bonded to one of the spheres and the center line of the rubber layer. Ten elements of gradually increasing width were employed laterally, between the cylindrical axis and the free surface, as shown schematically in Figure 1. Values of stress were calculated by taking an average over four integration points of the eight-node axi-symmetric elements.

When an axial force $\underline{F}$ was applied to the spheres to compress or stretch the layer bonded between them, Figure 1, the FEM computations yielded corresponding values for the displacement $\underline{\delta}$, axial stress $\underline{\sigma_z}$, radial stress, $\underline{\sigma_r}$, tangential stress $\underline{\sigma_t}$, and hydrostatic tension, $-\underline{P}$, where

$$- P = (\sigma_z + \sigma_r + \sigma_t)/3 \qquad (2)$$

These results are reported here for a wide range of layer thicknesses and for various values of Poisson's ratio, $\underline{\nu}$.

3. Results and discussion

(i) Stiffness of a bonded layer

Values of the computed compression or tensile stiffness for a bonded rubber layer are plotted in Figure 2 against the corresponding value of Poisson's ratio for the rubber. They are given in reduced form, as the dimensionless ratio, $F/\delta DE$, for selected values of the ratio h/D of the distance h between the spheres to the sphere diameter D.

As the results given in Figure 2 show, the stiffness of thin layers is extremely sensitive to the value of Poisson's ratio, even when it is quite close to 0.5, corresponding to complete incompressibility. For example, for a layer with a thickness ratio h/D of 0.01, the stiffness is reduced by nearly 70 percent in comparison with the result for an incompressible material, when ν = 0.45. Even for a value of ν of 0.49, close to the incompressibility limit, the computed stiffness is still about 40 percent less than the value for a truly incompressible material. On the other hand, the stiffness of thicker layers is much less sensitive to small departures from complete incompressibility (Figure 2).

By extrapolation to ν = 0.5, values of the stiffness of thin layers were obtained for comparison with those deduced previously from an approximate theoretical treatment for incompressible layers (1):

$$F/\delta DE = (\pi/8)\left[A\ln[A/(A-1)] - 1 + (1/2A) + [1/(A-1)] \right] \qquad (3)$$

where $A = 1 + (h/D)$. This comparison is made in Table 1 and Figure 3. The extrapolated results are seen to be in close agreement with the approximate theory over the entire range of rubber layer thickness. The maximum difference is about 6% , when the rubber layer thickness is relatively large, $h/D = 0.2$. Thus, the approximate theory is surprisingly successful in predicting the stiffness of thin incompresible rubber layers.

Because the approximate theory gave results in good agreement with experimentally-measured compression stiffnesses for bonded rubber layers (1), we can conclude that the numerical calculations are also in good agreement with experiment. This comparison is included in Figure 3.

(ii) Stress distribution within the layer

Values of the hydrostatic pressure $\underline{P}$ for compressed layers, or triaxial tension (negative hydrostatic pressure) for layers subjected to tensile loads, were computed by FEM, using Equation 2. Maximum values were found to be developed on the central axis. Results for the layer center are plotted in Figure 4 against the value of Poisson's ratio, $\underline{\nu}$, of the rubber. They are seen to be quite sensitive to small departures from complete incompressibility, especially for thin layers,as found before for the layer stiffness, Figure 2. (Note that logarithmic scales are employed in Figure 4, in view of the wide range of pressures encountered.) And, again, the results for thicker rubber layers were less sensitive to the exact value of Poisson's ratio.

By extrapolating to a value for $\underline{\nu}$ of 0.5, corresponding to a completely incompressible rubber layer, results were obtained for direct comparison with the predictions of the approximate theoretical analysis (1), where the total pressure is assumed to be made up of two components, the first given by simple compression of an (unbonded) incompessible layer

$$P_1 = E\delta/3h \tag{4}$$

and the second arising from restraints at the bonded interfaces

$$P_2 = E\delta/4AD(A-1)^2 \tag{5}$$

where $\underline{\delta}$ is the displacement, calculated from the total stiffness, Equation 3.

This comparison is made in Figure 5. Good agreement is seen to hold between values of pressure at the layer center, calculated from FEM and from the approximate theory.

Thus, the approximate theory is apparently able to predict the pressures set up in thin incompressible layers with surprising accuracy.

Up to this point, pressure were evaluated by FEM at the center of the elastic layer, for comparison with predictions of the simple approximate theory. But the FEM calculations revealed that, although maximum pressures were, indeed, developed on the central axis, they were not generally constant through the layer thickness. When the layer was extremely thin, the pressure was approximately uniform between the two spheres, Figure 6. But when the layer was thicker; for example, when $\underline{h/D = 0.1}$; then the hydrostatic tension near the bonded interfaces was significantly larger than in the center of the layer, Figure 6. Thus, for thin layers, failure due to the action of a hydrostatic tension could occur at any point along the axis between the two spheres, whereas for thicker layers it is more likely to take place near the bonded surfaces. Experimental studies have shown that the first cavity appears in relatively thick layers near the bonded interfaces (2).

(iii) Anisotropy of stresses

FEM computations also revealed that the principal stresses set up along the center line were not strictly equal. They approached pure triaxiality for thin layers but for moderately thick ones the axial stress at the center of the layer was considerably larger than the radial and tangential stresses (which were roughly equal), Figure 7. However, near the bonded surfaces the stresses remained substantially equal, even for thick layers.

We conclude that failure by growth of a pre-existing cavity at a critical level of triaxial tension will occur first near the bonded surfaces for moderately thick layers, $\underline{h/D} \doteq 0.1$, and somewhat later, i.e., at a higher applied load, in the central region of the rubber layer, as observed experimentally (2). But the nature of the second fracture, and in particular the direction of tear propagation, is likely to be somewhat different because the stress field is not isotropic.

Conclusions

Stiffnesses calculated by FEM for thin incompressible rubber layers sandwiched between, and bonded to, two rigid spheres are in good agreement with a previously-derived approximate theory and with experimental measurements of compression stiffness. However, the calculated stiffnesses of thin layers are extremely sensitive to the value chosen for Poisson's ratio. Small departures from complete incompressibility bring about large reductions in stiffness.

The highest level of pressure in compression, or dilatant stress (triaxial tension) in tension, is developed at points near the bonded surfaces of the spheres for moderately thick rubber layers. This is the place at which an initial cavity appears when bonded rubber layers are subjected to tension (2).

Calculations of the radial and tangential stress show that the stresses in the center are strictly triaxial only for thin layers. For thicker layers, the axial tensile stress is substantially greater than the lateral stresses. This feature of the stress distribution has implications for the direction of tearing when an initial cavity forms at the center of the rubber layer. The tear will presumably run at right angles to the major tensile stress; that is, across the axis of symmetry; and this is the direction observed in practice (2). On the other hand, cavities formed near the bonded surfaces are in an isotropic stress field with no preferred direction. In practice, they propagate along the axis and thus do not lead directly to failure of the bonded structure.

Acknowledgements

This work was supported in part by the Office of Naval Research (Contract N00014-85-K-0222) and in part by a grant-in-aid from Lord Corporation. The authors are also indebted to Professor R.A.Schapery of Texas A and M University for helpful suggestions on the analysis of bonded layers.

References

1. A.N.Gent and B.Park, Rubber Chem.Technol. 59, 77 (1986).

2. A.N.Gent and B.Park, J. Materials Sci. 19, 1947 (1984).

3. P.B.Lindley, "Engineering Design With Natural Rubber", 3rd. Ed., NR Technical Bulletin, Natural Rubber Producer's Research Association, London, 1970.

4. A.N.Gent and P.B.Lindley, Proc.Roy.Soc.(London) A249, 195 (1958).

5 A.E.Oberth and R.S.Bruenner, Trans.Soc.Rheol. 9, 165 (1965).

6. A.N.Gent and D.A.Tompkins, J.Appl.Phys. 40, 2520 (1969).

7. K.J.Bathe, "ADINA: A Finite Element Program for Automatic Dynamic Nonlinear Incremental Analysis," Report No. 82448-1, Mass. Inst. Technol., Cambridge, Mass., 1977.

Table 1: Stiffness, $F/\delta DE$ for an incompressible elastic layer bonded between two spheres of diameter D and initial separation h.

h/D	$F/\delta DE$ from FEM	$F/\delta DE$ from approximate theory (1)	Difference (per cent)
0.01	40.77	40.90	0.32
0.02	20.916	21.01	0.45
0.05	8.704	8.904	2.24
0.1	4.519	4.749	4.84
0.2	2.399	2.579	6.96
0.5	1.122	1.171	4.13
1	0.648	0.643	-0.86
2	0.358	0.347	-3.32

Figure Legends

Figure 1. Sketch of the model employed for FEM calculations.

Figure 2. Calculated stiffness F/δ plotted against the value of Poisson's ratio ν, for various thicknesses h of the elastic layer relative to the sphere diameter D.

Figure 3. Stiffness F/δ plotted against the layer thickness h, relative to the sphere diameter D. The open circles represent the results of FEM calculations for an incompressible material. The filled-in circles are experimentally-measured values for a silicone rubber layer, E = 2 MPa, (1). The full line represents the results of a previous approximate theory (1).

Figure 4. Pressure P_c, developed at the center of an elastic layer, plotted against the value of Poisson's ratio ν, for various values of the layer thickness h, relative to the sphere diameter D. P_o denotes the mean applied stress, given by $4F/\pi D^2$.

Figure 5. Pressure P_c, developed at the center of an incompressible elastic layer, plotted against the layer thickness h relative to the sphere diameter D. P_o denotes the mean applied stress, given by $4F/\pi D^2$. The full curve represents the predictions of a previous approximate theory (1). The points represent values calculated by FEM.

Figure 6. Pressure P developed along the central axis, plotted

against the distance z from the center of an incompressible elastic layer of thickness h. The point $z = h/2$ is at the bonded interface. P_c denotes the pressure set up at the center of the layer.

Figure 7. Ratio of the radial stress σ_r to the axial stress σ_z, plotted against the distance z from the center of an incompressible elastic layer of thickness h.

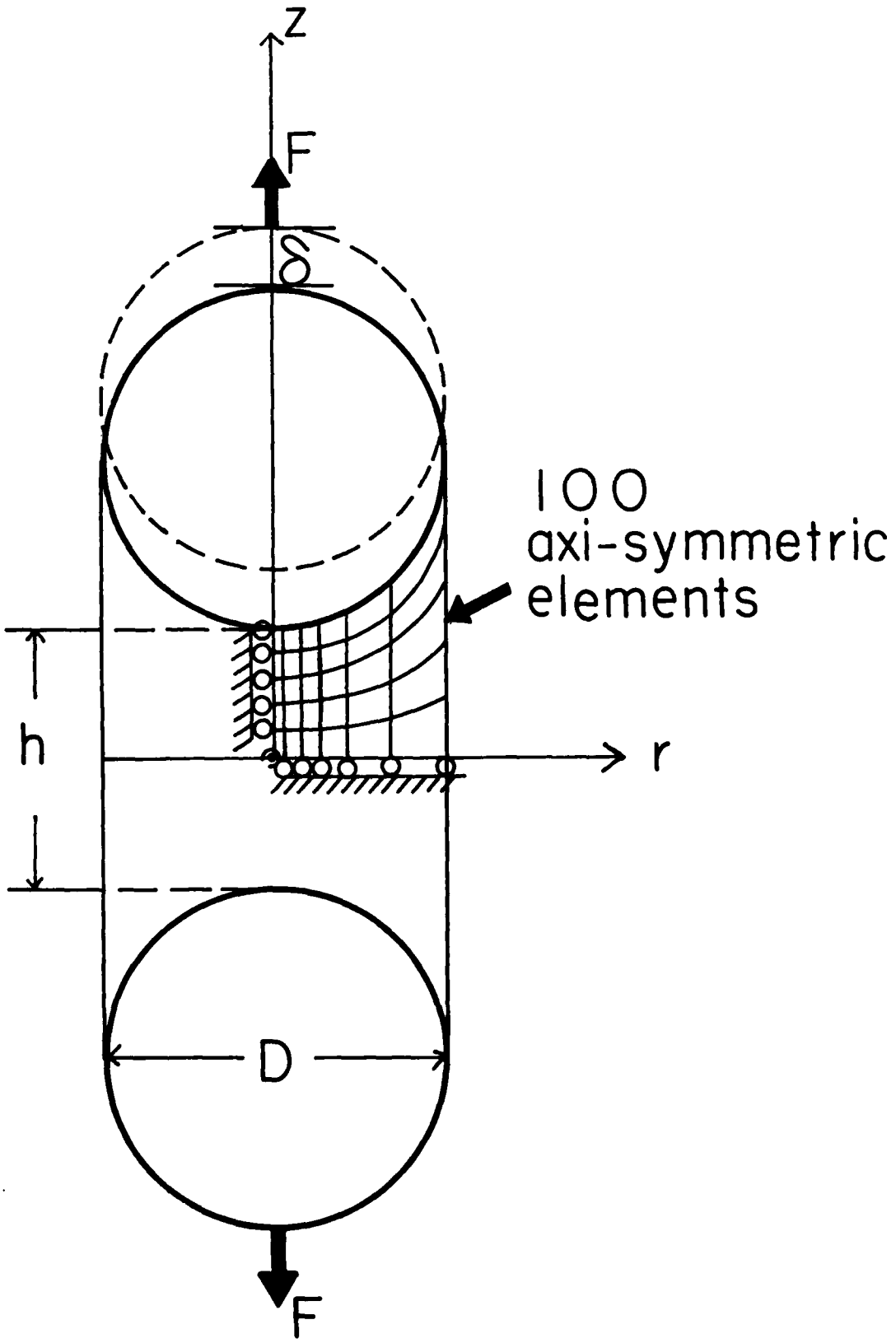

Figure 1

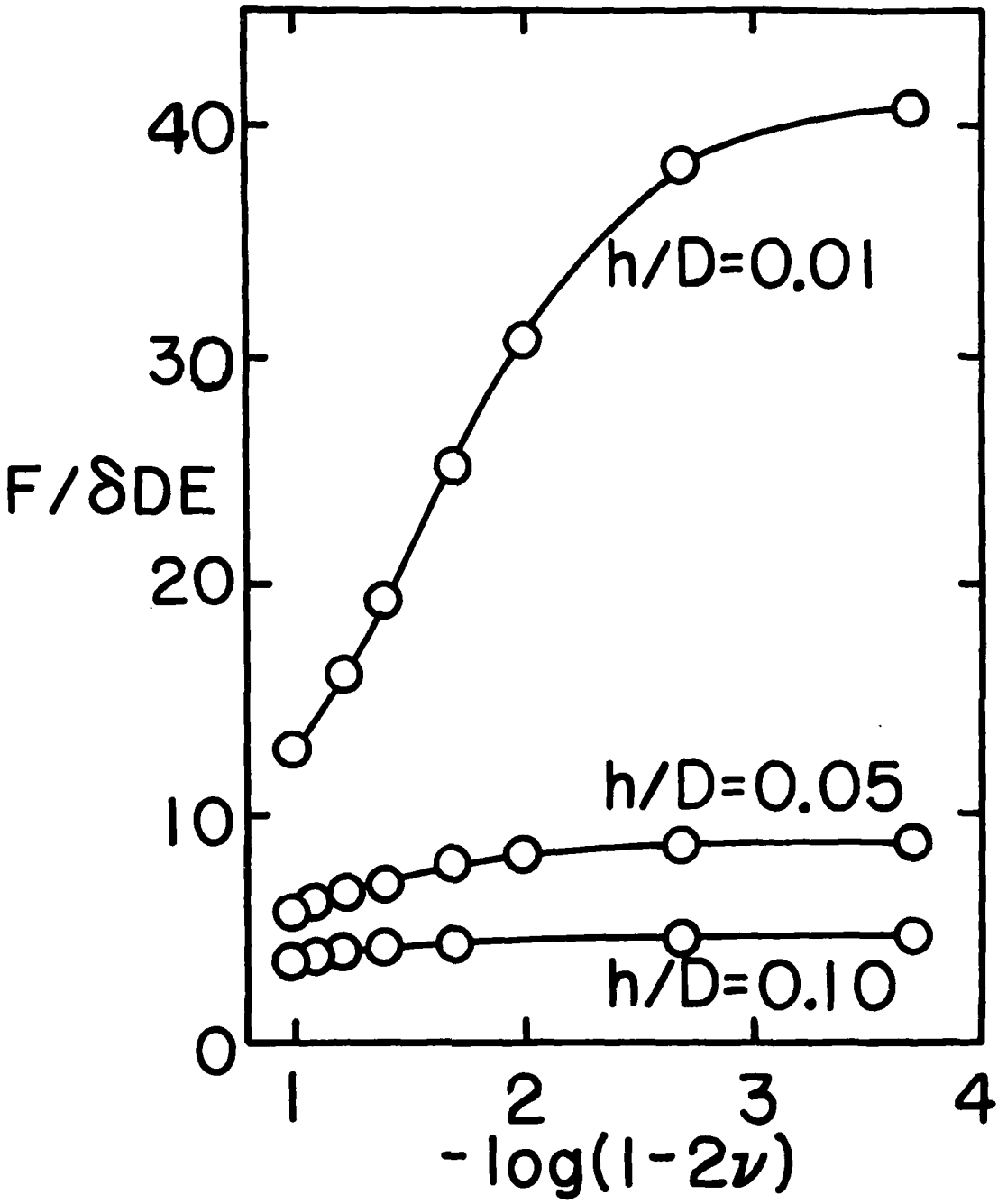

Figure 2

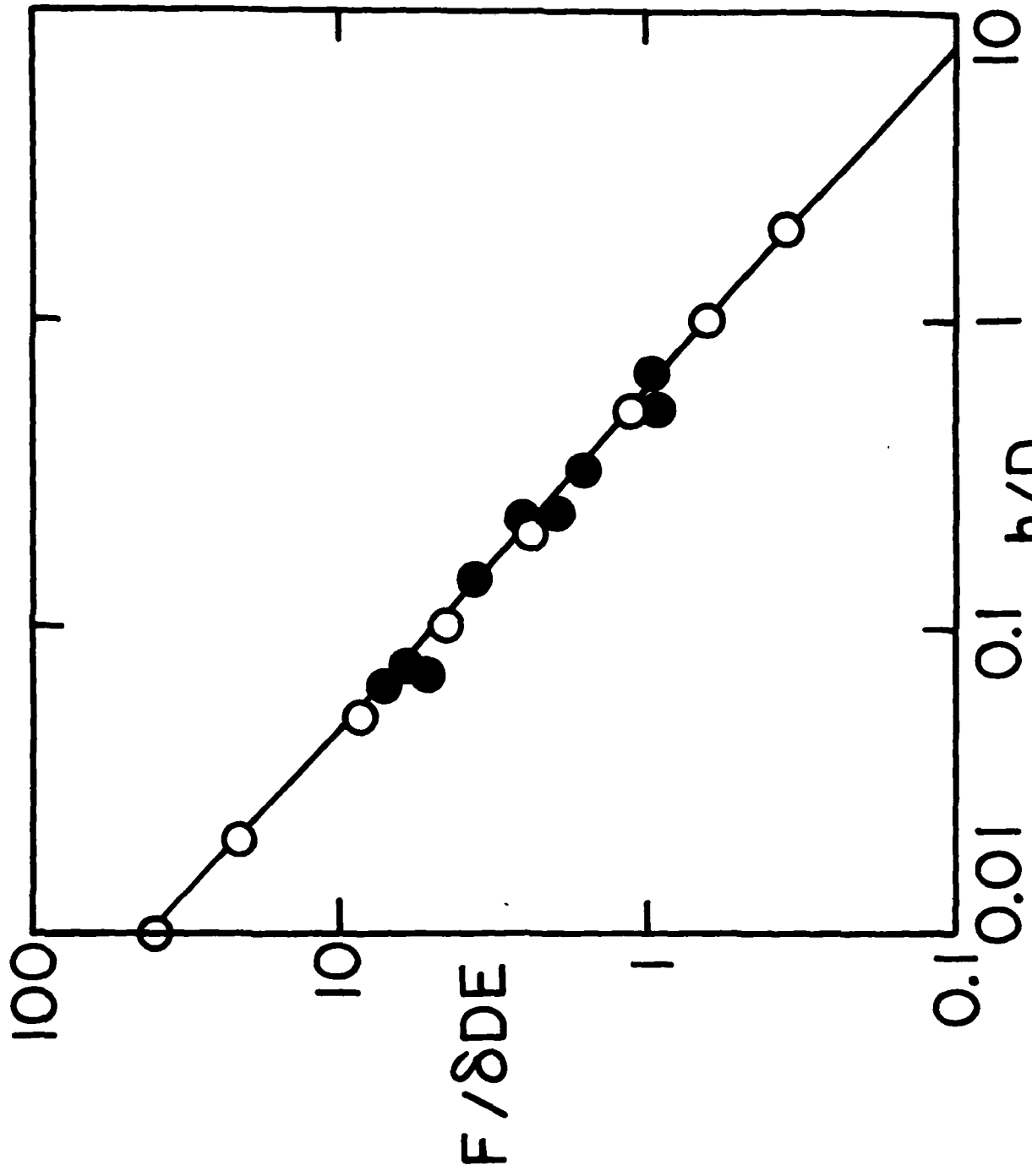

Figure 3

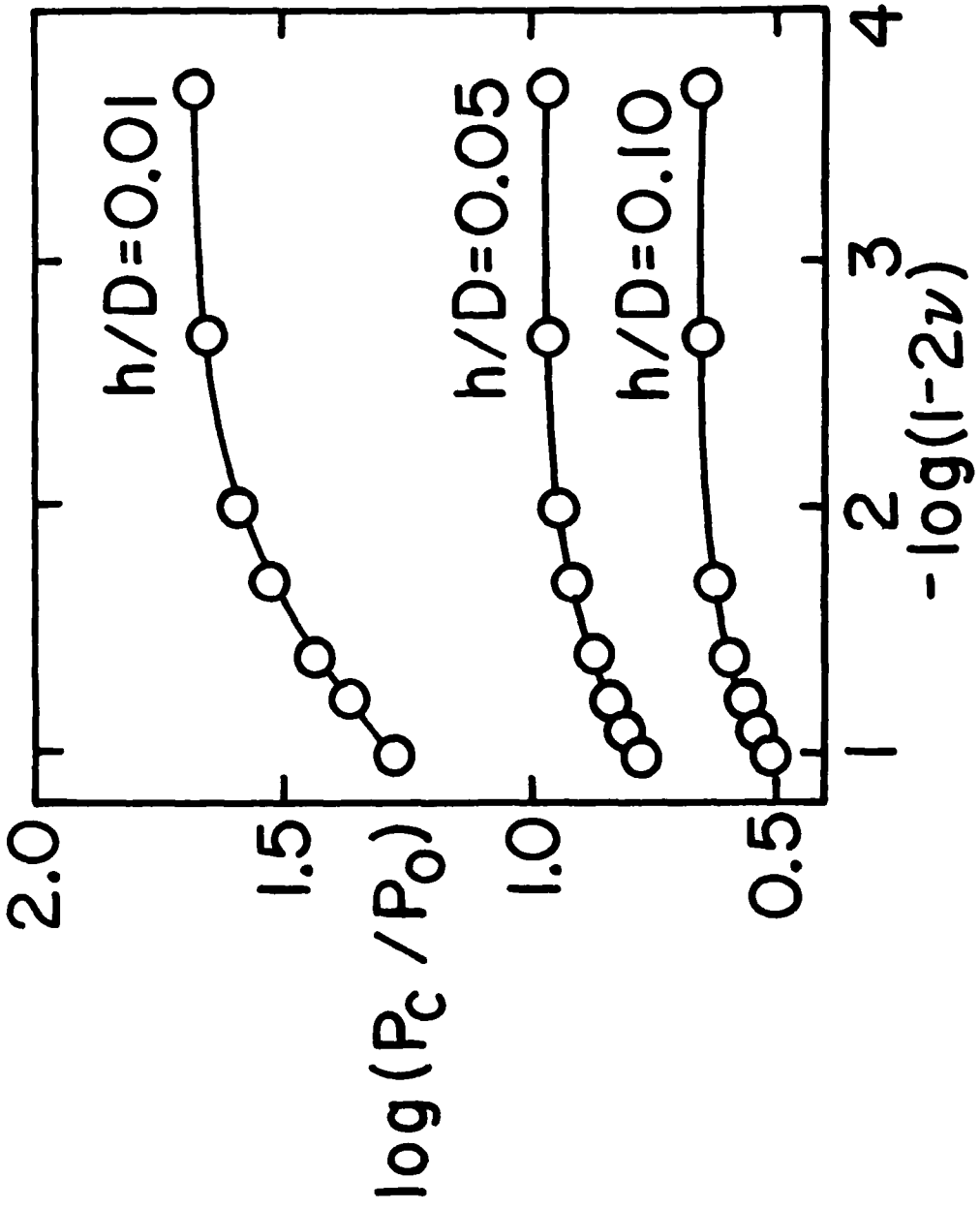

Figure 4

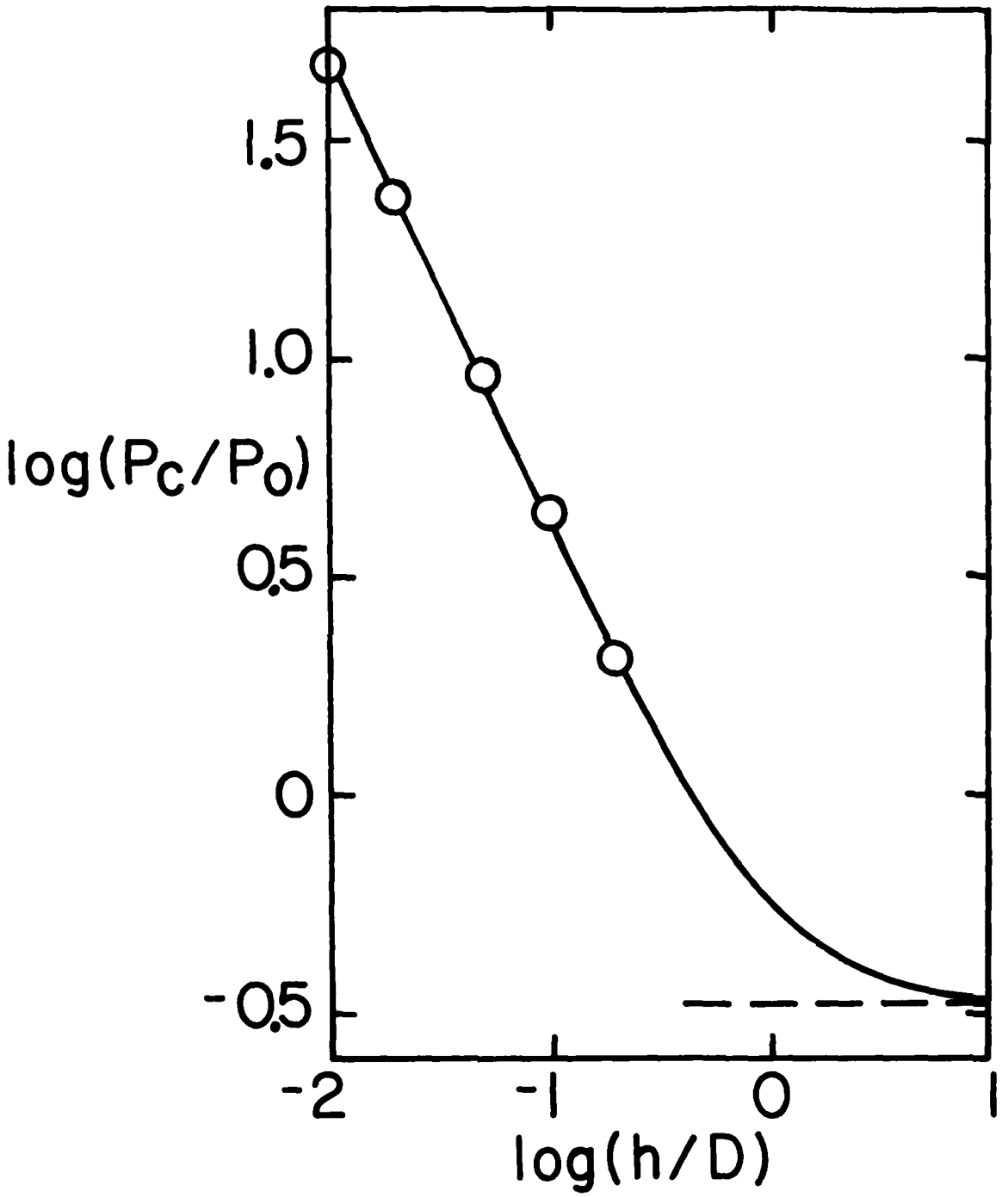

Figure 5

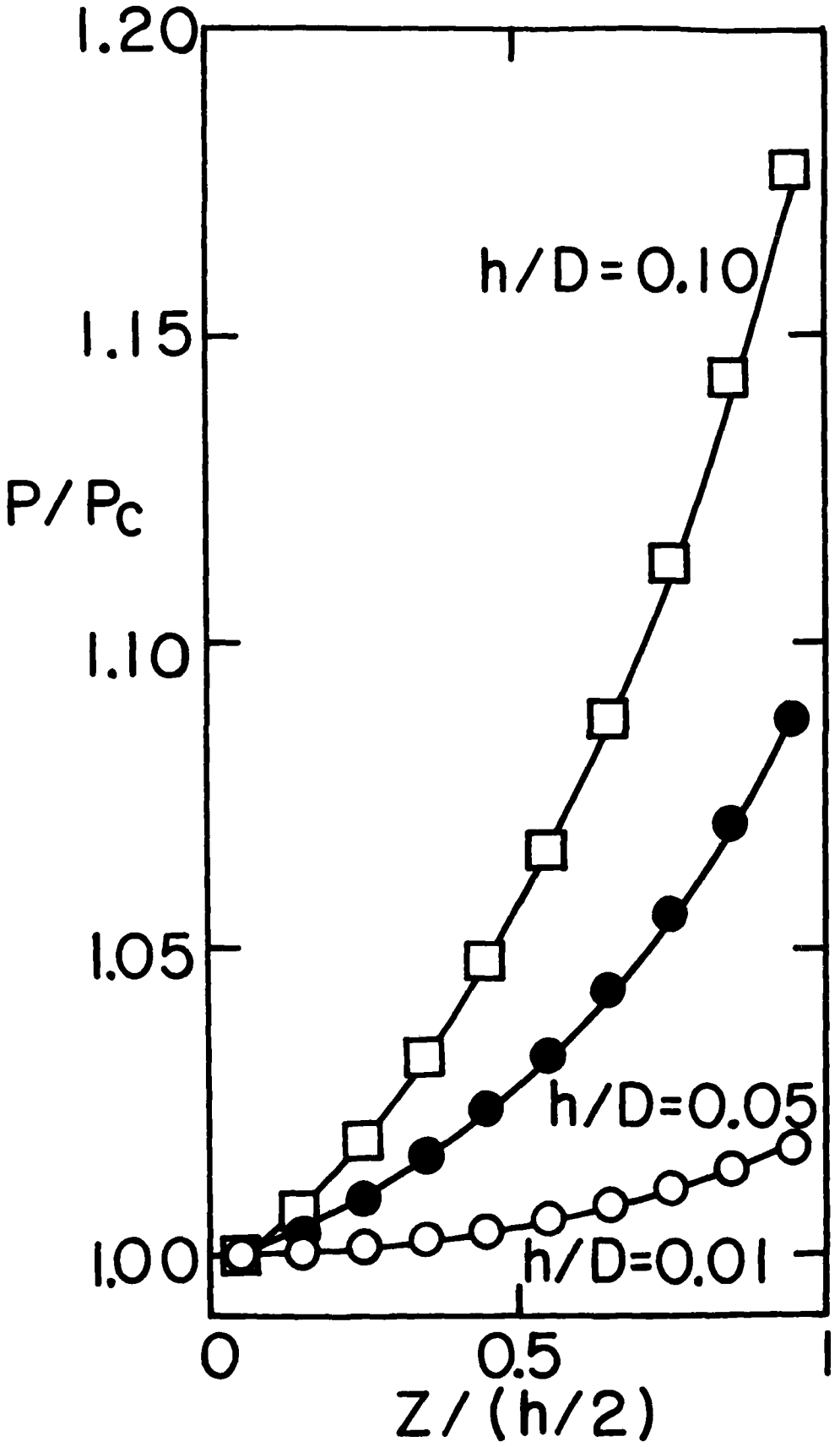

Figure 6

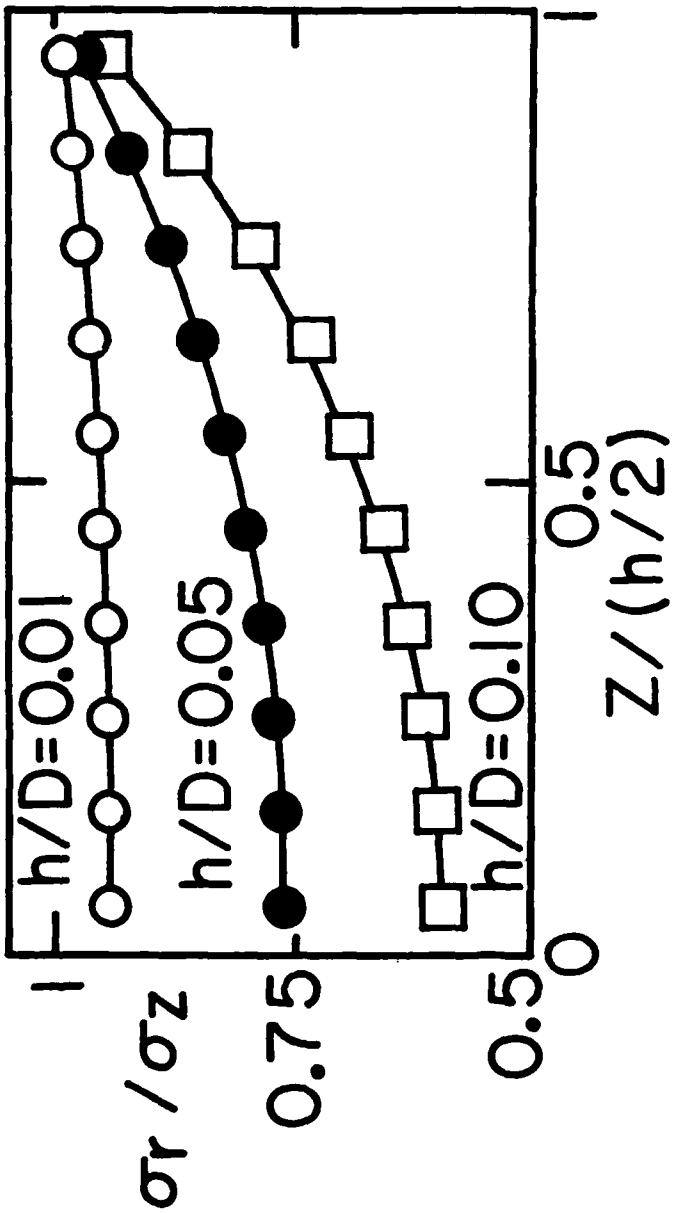

Figure 7

(DYN)

DISTRIBUTION LIST

Dr. R.S. Miller
Office of Naval Research
Code 432P
Arlington, VA 22217
(10 copies)

Dr. J. Pastine
Naval Sea Systems Command
Code 06R
Washington, DC 20362

Dr. Kenneth D. Hartman
Hercules Aerospace Division
Hercules Incorporated
Alleghany Ballistic Lab
P.O. Box 210
Cumberland, MD 20502

Mr. Otto K. Heiney
AFATL-DLJG
Elgin AFB, FL 32542

Dr. Merrill K. King
Atlantic Research Corp.
5390 Cherokee Avenue
Alexandria, VA 22312

Dr. R.L. Lou
Aerojet Strategic Propulsion Co.
Bldg. 05025 - Dept 5400 - MS 167
P.O. Box 15699C
Sacramenta, CA 95813

Dr. R. Olsen
Aerojet Strategic Propulsion Co.
Bldg. 05025 - Dept 5400 - MS 167
P.O. Box 15699C
Sacramento, CA 95813

Dr. Randy Peters
Aerojet Strategic Propulsion Co.
Bldg. 05025 - Dept 5400 - MS 167
P.O. Box 15699C
Sacramento, CA 95813

Dr. D. Mann
U.S. Army Research Office
Engineering Division
Box 12211
Research Triangle Park, NC 27709-2211

Dr. L.V. Schmidt
Office of Naval Technology
Code 07CT
Arlington, VA 22217

JHU Applied Physics Laboratory
ATTN: CPIA (Mr. T.W. Christian)
Johns Hopkins Rd.
Laurel, MD 20707

Dr. R. McGuire
Lawrence Livermore Laboratory
University of California
Code L-324
Livermore, CA 94550

P.A. Miller
736 Leavenworth Street, #6
San Francisco, CA 94109

Dr. W. Moniz
Naval Research Lab.
Code 6120
Washington, DC 20375

Dr. K.F. Mueller
Naval Surface Weapons Center
Code R11
White Oak
Silver Spring, MD 20910

Prof. M. Nicol
Dept. of Chemistry & Biochemistry
University of California
Los Angeles, CA 90024

Mr. L. Roslund
Naval Surface Weapons Center
Code R10C
White Oak, Silver Spring, MD 20910

Dr. David C. Sayles
Ballistic Missile Defense
Advanced Technology Center
P.O. Box 1500
Huntsville, AL 35807

(DYN)

DISTRIBUTION LIST

Mr. R. Geisler
ATTN: DY/MS-24
AFRPL
Edwards AFB, CA 93523

Naval Air Systems Command
ATTN: Mr. Bertram P. Sobers
NAVAIR-320G
Jefferson Plaza 1, RM 472
Washington, DC 20361

R.B. Steele
Aerojet Strategic Propulsion Co.
P.O. Box 15699C
Sacramento, CA 95813

Mr. M. Stosz
Naval Surface Weapons Center
Code R10B
White Oak
Silver Spring, MD 20910

Mr. E.S. Sutton
Thiokol Corporation
Elkton Division
P.O. Box 241
Elkton, MD 21921

Dr. Grant Thompson
Morton Thiokol, Inc.
Wasatch Division
MS 240 P.O. Box 524
Brigham City, UT 84302

Dr. R.S. Valentini
United Technologies Chemical Systems
P.O. Box 50015
San Jose, CA 95150-0015

Dr. R.F. Walker
Chief, Energetic Materials Division
DRSMC-LCE (D), B-3022
USA ARDC
Dover, NJ 07801

Dr. Janet Wall
Code 012
Director, Research Administration
Naval Postgraduate School
Monterey, CA 93943

Director
US Army Ballistic Research Lab.
ATTN: DRXBR-IBD
Aberdeen Proving Ground, MD 21005

Commander
US Army Missile Command
ATTN: DRSMI-RKL
Walter W. Wharton
Redstone Arsenal, AL 35898

Dr. Ingo W. May
Army Ballistic Research Lab.
ARRADCOM
Code DRXBR - 1BD
Aberdeen Proving Ground, MD 21005

Dr. E. Zimet
Office of Naval Technology
Code 071
Arlington, VA 22217

Dr. Ronald L. Derr
Naval Weapons Center
Code 389
China Lake, CA 93555

T. Boggs
Naval Weapons Center
Code 389
China Lake, CA 93555

Lee C. Estabrook, P.E.
Morton Thiokol, Inc.
P.O. Box 30058
Shreveport, Louisiana 71130

Dr. J.R. West
Morton Thiokol, Inc.
P.O. Box 30058
Shreveport, Louisiana 71130

Dr. D.D. Dillehay
Morton Thiokol, Inc.
Longhorn Division
Marshall, TX 75670

G.T. Bowman
Atlantic Research Corp.
7511 Wellington Road
Gainesville, VA 22065

(DYN)

DISTRIBUTION LIST

R.E. Shenton
Atlantic Research Corp.
7511 Wellington Road
Gainesville, VA 22065

Brian Wheatley
Atlantic Research Corp.
7511 Wellington Road
Gainesville, VA 22065

Mike Barnes
Atlantic Research Corp.
7511 Wellington Road
Gainesville, VA 22065

Mr. G. Edwards
Naval Sea Systems Command
Code 62R32
Washington, DC 20362

Dr. Lionel Dickinson
Naval Explosive Ordinance
Disposal Tech. Center
Code D
Indian Head, MD 20340

C. Dickinson
Naval Surface Weapons Center
White Oak, Code R-13
Silver Spring, MD 20910

Prof. J.T. Dickinson
Washington State University
Dept. of Physics 4
Pullman, WA 99164-2814

Prof. John Deutch
MIT
Department of Chemistry
Cambridge, MA 02139

M.H. Miles
Dept. of Physics
Washington State University
Pullman, WA 99164-2814

Dr. E.H. deButts
Hercules Aerospace Co.
P.O. Box 27408
Salt Lake City, UT 84127

Dr. T.F. Davidson
Vice President, Technical
Morton Thiokol, Inc.
Aerospace Group
3340 Airport Rd.
Ogden, UT 84405

David A. Flanigan
Director, Advanced Technology
Morton Thiokol, Inc.
Aerospace Group
3340 Airport Rd.
Ogden, UT 84405

Mr. J. Consaga
Naval Surface Weapons Center
Code R-16
Indian Head, MD 20640

Dr. L.H. Caveny
Air Force Office of Scientific
Research
Directorate of Aerospace Sciences
Bolling Air Force Base
Washington, DC 20332

Naval Sea Systems Command
ATTN: Mr. Charles M. Christensen
NAVSEA-62R2
Crystal Plaza, Bldg. 6, Rm 806
Washington, DC 20362

W.G. Roger
Code 5253
Naval Ordance Station
Indian Head, MD 20640

Mr. R. Beauregard
Naval Sea Systems Command
SEA 64E
Washington, DC 20362

Dr. Donald L. Ball
Air Force Office of Scientific
Research
Directorate of Chemical &
Atmospheric Sciences
Bolling Air Force Base
Washington, DC 20332

(DYN)

DISTRIBUTION LIST

Dr. Anthony J. Matuszko
Air Force Office of Scientific Research
Directorate of Chemical & Atmospheric Sciences
Bolling Air Force Base
Washington, DC 20332

Dr. Michael Chaykovsky
Naval Surface Weapons Center
Code R11
White Oak
Silver Spring, MD 20910

J.J. Rocchio
USA Ballistic Research Lab.
Aberdeen Proving Ground, MD 21005-5066

B. Swanson
INC-4 MS C-346
Los Alamos National Laboratory
Los Alamos, New Mexico 87545

Dr. James T. Bryant
Naval Weapons Center
Code 3205B
China Lake, CA 93555

Dr. L. Rothstein
Assistant Director
Naval Explosives Dev. Engineering Dept.
Naval Weapons Station
Yorktown, VA 23691

Dr. M.J. Kamlet
Naval Surface Weapons Center
Code R11
White Oak, Silver Spring, MD 20910

Dr. Henry Webster, III
Manager, Chemical Sciences Branch
ATTN: Code 5063
Crane, IN 47522

Dr. A.L. Slafkosky
Scientific Advisor
Commandant of the Marine Corps
Code RD-1
Washington, DC 20380

Dr. H.G. Adolph
Naval Surface Weapons Center
Code R11
White Oak
Silver Spring, MD 20910

U.S. Army Research Office
Chemical & Biological Sciences Division
P.O. Box 12211
Research Triangle Park, NC 27709

Dr. John S. Wilkes, Jr.
FJSRL/NC
USAF Academy, CO 80840

Dr. H. Rosenwasser
AIR-320R
Naval Air Systems Command
Washington, DC 20361

Dr. Joyce J. Kaufman
The Johns Hopkins University
Department of Chemistry
Baltimore, MD 21218

Dr. A. Nielsen
Naval Weapons Center
Code 385
China Lake, CA 93555

(DYN)

DISTRIBUTION LIST

K.D. Pae
High Pressure Materials Research Lab.
Rutgers University
P.O. Box 909
Piscataway, NJ 08854

Dr. John K. Dienes
T-3, B216
Los Alamos National Lab.
P.O. Box 1663
Los Alamos, NM 87544

A.N. Gent
Institute Polymer Science
University of Akron
Akron, OH 44325

Dr. D.A. Shockey
SRI International
333 Ravenswood Ave.
Menlo Park, CA 94025

Dr. R.B. Kruse
Morton Thiokol, Inc.
Huntsville Division
Huntsville, AL 35807-7501

G. Butcher
Hercules, Inc.
P.O. Box 98
Magna, UT 84044

W. Waesche
Atlantic Research Corp.
7511 Wellington Road
Gainesville, VA 22065

Dr. R. Bernecker
Naval Surface Weapons Center
Code R13
White Oak
Silver Spring, MD 20910

Prof. Edward Price
Georgia Institute of Tech.
School of Aerospace Engineering
Atlanta, GA 30332

J.A. Birkett
Naval Ordnance Station
Code 5253K
Indian Head, MD 20640

Prof. R.W. Armstrong
University of Maryland
Dept. of Mechanical Engineering
College Park, MD 20742

Herb Richter
Code 385
Naval Weapons Center
China Lake, CA 93555

J.T. Rosenberg
SRI International
333 Ravenswood Ave.
Menlo Park, CA 94025

G.A. Zimmerman
Aeroject Tactical Systems
P.O. Box 13400
Sacramento, CA 95813

Prof. Kenneth Kuo
Pennsylvania State University
Dept. of Mechanical Engineering
University Park, PA 16802

T.L. Boggs
Naval Weapons Center
Code 3891
China Lake, CA 93555

(DYN)

DISTRIBUTION LIST

Dr. C.S. Coffey
Naval Surface Weapons Center
Code R13
White Oak
Silver Spring, MD 20910

D. Curran
SRI International
333 Ravenswood Avenue
Menlo Park, CA 94025

E.L. Throckmorton
Code SP-2731
Strategic Systems Program Office
Crystal Mall #3, RM 1048
Washington, DC 23076

R.G. Rosemeier
Brimrose Corporation
7720 Belair Road
Baltimore, MD 20742

C. Gotzmer
Naval Surface Weapons Center
Code R-11
White Oak
Silver Spring, MD 20910

G.A. Lo
3251 Hanover Street
B204 Lockheed Palo Alto Research Lab
Palto Alto, CA 94304

R.A. Schapery
Civil Engineering Department
Texas A&M University
College Station, TX 77843

Dr. Y. Gupta
Washington State University
Department of Physics
Pullman, WA 99163

J.M. Culver
Strategic Systems Projects Office
SSPO/SP-2731
Crystal Mall #3, RM 1048
Washington, DC 20376

Prof. G.D. Duvall
Washington State University
Department of Physics
Pullman, WA 99163

Dr. E. Martin
Naval Weapons Center
Code 3858
China Lake, CA 93555

Dr. M. Farber
135 W. Maple Avenue
Monnovia, CA 91016

W.L. Elban
Naval Surface Weapons Center
White Oak, Bldg. 343
Silver Spring, MD 20910

Defense Technical Information Center
Bldg. 5, Cameron Station
Alexandria, VA 22314
(12 copies)

Dr. Robert Polvani
National Bureau of Standards
Metallurgy Division
Washington, D.C. 20234

Director
Naval Research Laboratory
Attn: Code 2627
Washington, DC 20375
(6 copies)

Administrative Contracting
Officer (see contract for
address)
(1 copy)

END
DATE
FILMED
7-88
DTIC